Monthly Notices
of the
ROYAL ASTRONOMICAL SOCIETY

Mon. Not. R. Astron. Soc. **406,** 1014–1028 (2010) doi:10.1111/j.1365-2966.2010.16723.x

The matter bispectrum in *N*-body simulations with non-Gaussian initial conditions

E. Sefusatti,[1⋆] M. Crocce[2⋆] and V. Desjacques[3⋆]

[1]*Institut de Physique Théorique, CEA, IPhT, F-91191 Gif-sur-Yvette, France*
[2]*Institut de Ciències de l'Espai, IEEC-CSIC, Campus UAB, Facultat de Ciències, Torre C5 par-2, Barcelona 08193, Spain*
[3]*Institute for Theoretical Physics, Universität Zürich, Winterthurerstrasse 190, CH-8057 Zürich, Switzerland*

Accepted 2010 March 22. Received 2010 March 19; in original form 2010 March 13

ABSTRACT

We present measurements of the dark matter bispectrum in *N*-body simulations with non-Gaussian initial conditions of the local kind for a large variety of triangular configurations and compare them with predictions from Eulerian perturbation theory up to one-loop corrections. We find that the effects of primordial non-Gaussianity at large scales, when compared to perturbation theory, are well described by the initial component of the matter bispectrum, linearly extrapolated at the redshift of interest. In addition, we find that for $f_{\rm NL} = 100$, the non-linear corrections *due* to non-Gaussian initial conditions are of the order of ∼3–4 per cent for generic triangles and up to ∼20 per cent for squeezed configurations, *at any redshift*. We show that the predictions of perturbation theory at the tree level fail to describe the simulation results at redshift $z = 0$ at scales corresponding to $k \sim 0.02$–$0.08\,h\,{\rm Mpc}^{-1}$, depending on the triangle, while one-loop corrections can significantly extend their validity to smaller scales. At higher redshift, one-loop perturbation theory indeed provides quite accurate predictions, particularly with respect to the *relative* correction due to primordial non-Gaussianity.

Key words: cosmology: theory – large-scale structure of the Universe.

1 INTRODUCTION

In recent years, a significant research activity has been devoted to the effects of a possible small departure from Gaussianity in the primordial cosmological perturbations. While current constraints on primordial non-Gaussianity from measurements of the cosmic microwave background (CMB) and the large-scale structure are still consistent with the Gaussian hypothesis (Slosar et al. 2008; Komatsu et al. 2010), a possible detection in forthcoming experiments would constitute a major discovery, providing crucial information on the early Universe and on the high-energy physics of inflation (see, for instance, Komatsu et al. 2009a).

The effect of primordial non-Gaussianity on the large-scale structure has been assumed, for a long time, to be limited to an additional, *primordial* component to the matter skewness and bispectrum induced by gravitational instability and to a correction to the abundance of a massive cluster [see Liguori et al. (2010); Desjacques & Seljak (2010b) for recent reviews]. Numerical and analytical studies have indeed shown that a matter density probability distribution initially skewed towards positive values produces more overdense regions and, consequently, collapsed objects while a negatively skewed distribution produces larger voids (see Grossi et al. 2008; Kamionkowski, Verde & Jimenez 2009; Lam & Sheth 2009; Lam, Sheth & Desjacques 2009; Maggiore & Riotto 2009; Pillepich, Porciani & Hahn 2010, for recent work). Moreover, a non-vanishing skewness in the initial conditions corresponds to a primordial component to the matter bispectrum, i.e. the three-point function in Fourier space. For the *local* non-Gaussian model considered here, the primordial matter bispectrum exhibits a scale, redshift and triangle shape dependence distinct from that of the component sourced by the non-linear growth of structures. This enables us in principle to disentangle the two contributions. In the specific case of equilateral triangular configurations, the primordial contribution to the matter bispectrum scales as $\sim k^{-2}$ relative to the gravity-induced term, leading to large, potentially observable corrections at low wavenumbers. Measurements of the galaxy bispectrum in future large-volume redshift surveys (such as Euclid or HETDEX) should be able to provide constraints on the local non-Gaussian model competitive with those from CMB observations (Scoccimarro, Sefusatti & Zaldarriaga 2004; Sefusatti & Komatsu 2007; Sefusatti et al. 2009).

In addition to these effects, Dalal et al. (2008) have recently discovered a large correction to the galaxy bias in numerical simulations of *local* primordial non-Gaussianity. Further numerical and theoretical work has confirmed this result (Afshordi & Tolley 2008; Grossi et al. 2008; McDonald 2008; Matarrese & Verde 2008; Slosar et al. 2008; Taruya, Koyama & Matsubara 2008; Desjacques, Seljak & Iliev 2009; Giannantonio & Porciani 2010; Pillepich et al. 2010).

⋆E-mail: emiliano.sefusatti@cea.fr (ES); crocce@ieec.uab.es (MC); dvince@physik.uzh.ch (VD)

© 2010 The Authors. Journal compilation © 2010 RAS

The constraints obtained from the power spectrum measurement of highly biased objects in current data sets are already comparable to the CMB results (Slosar et al. 2008; Desjacques & Seljak 2010a), and the prospects for detecting local primordial non-Gaussianity with galaxy clustering look exciting (Carbone, Verde & Matarrese 2008; Dalal et al. 2008; Seljak 2009; Slosar 2009; Verde & Matarrese 2009; Desjacques & Seljak 2010a). At this point, analyses of the galaxy bispectrum preceding the work of Dalal et al. (2008) must be updated to account for the non-Gaussian correction to the galaxy bias. In fact, a rigorous *joint* analysis of the galaxy power spectrum and bispectrum in presence of local non-Gaussianity is in order. First steps in this direction have been taken by Jeong & Komatsu (2009) and Sefusatti (2009) with a preliminary comparison with simulations in Nishimichi et al. (2009).

In this perspective, we will consider the measurement of several triangular configurations of the *matter* bispectrum on mildly non-linear scales, with both Gaussian and non-Gaussian initial conditions of the local type. Although the matter bispectrum is not directly observable with tracers of the large-scale structure, it is instructive to assess the extent to which perturbation theory (PT) describes the shape dependence of the matter three-point function in the presence of non-Gaussianity of the local type. This analysis will be useful when considering the complication brought by biasing, which will be addressed in a forthcoming publication. Measurements of the matter power spectrum with local non-Gaussianity can be found in Pillepich et al. (2010) and Desjacques et al. (2009), where the small corrections at mildly non-linear scales predicted in the framework of PT by Taruya et al. (2008) are observed. In the case of the matter bispectrum, measurements in simulations with Gaussian initial conditions are shown in Scoccimarro et al. (1998), Hou et al. (2005), Pan, Coles & Szapudi (2007), Smith, Sheth & Scoccimarro (2008) and Guo & Jing (2009), with Smith et al. (2008) considering, in addition, redshift space predictions in the context of the halo model. By contrast, the only measurement so far of the matter (and halo) bispectrum in simulations with local non-Gaussian initial conditions can be found in Nishimichi et al. (2009), where a relatively small subset of isosceles triangular configurations is considered.

We will compare our measurements with predictions of the matter bispectrum at the one-loop approximation in Eulerian PT. A comparison of one-loop results with the bispectrum extracted from simulations with Gaussian initial conditions is shown in Scoccimarro et al. (1998), whereas a comparison of the effect of primordial non-Gaussianity with the tree-level prediction of PT is performed in Nishimichi et al. (2009) for 'squeezed' isosceles configurations at $z = 0$ with $k \lesssim 0.1\,h\,\mathrm{Mpc}^{-1}$ only. Here, we will extend the analysis to include several triangular configurations covering the range of scales $0.002 \lesssim k \lesssim 0.3\,h\,\mathrm{Mpc}^{-1}$ and redshifts $z = 0, 1$ and 2. This will allow us to broadly test the accuracy of one-loop PT in the mildly non-linear regime. We will also discuss the validity of two phenomenological prescriptions for the non-linear bispectrum with Gaussian initial conditions, namely the fitting function of Scoccimarro & Couchman (2001) and the formula of Pan et al. (2007) based on a scaling transformation.

This paper is organized as follows. In Section 2, we summarize previous results on the predictions of the matter power spectrum and bispectrum in cosmological PT for both Gaussian and local non-Gaussian initial perturbations. In Section 3 we describe the N-body simulations and the bispectrum estimator employed in our analysis, whereas in Section 4 we present our measurements of the matter bispectrum and compare them to one-loop predictions in PT. Finally, we conclude in Section 5.

2 THEORY

In this section, we summarize previous results on the non-linear evolution of the matter correlators as described specifically by Eulerian PT. The quantity of interest, the matter overdensity δ, is obtained as a perturbative solution to the continuity and Euler equations and the Poisson equation relating matter perturbations and the gravitational potential. These equations fully determine the evolution of the matter density and velocity fields, once the initial conditions are given in terms of the primordial correlators. Other approaches such as Lagrangian PT, for instance, have also been studied in the literature. We refer the reader to Scoccimarro (2000) for a study of the matter bispectrum in Lagrangian PT with Gaussian initial conditions and to Bernardeau et al. (2002) for a complete review of cosmological PT.

2.1 Initial conditions

Our N-body simulations of the matter density evolution assume *local* non-Gaussian initial conditions. This model of primordial non-Gaussianity is defined by the *local* expression in position space for Bardeen's curvature perturbations Φ (Salopek & Bond 1990, 1991; Gangui et al. 1994; Verde et al. 2000; Komatsu & Spergel 2001):

$$\Phi(\boldsymbol{x}) = \phi(\boldsymbol{x}) + f_{\mathrm{NL}}[\phi^2(\boldsymbol{x}) - \langle\phi^2(\boldsymbol{x})\rangle], \tag{1}$$

where the second term on the rhs represents a non-Gaussian correction to the Gaussian random field $\phi(\boldsymbol{x})$. In this expression, we assume that $\phi(\boldsymbol{x})$ is the curvature field during early matter domination and not the linearly extrapolated value at present time. Despite its relatively simple form, the parametrization of primordial non-Gaussianity provided by equation (1) well describes inflationary models in which the non-Gaussianity is produced by local mechanisms on superhorizon scales (see Bartolo et al. 2004; Liguori et al. 2010; Chen 2010; Byrnes & Choi 2010, and references therein).

The definition of equation (1) corresponds to a very specific functional form of the bispectrum and trispectrum of the initial curvature perturbations. One finds the following leading contribution to the curvature bispectrum:

$$B_\Phi(k_1, k_2, k_3) = 2 f_{\mathrm{NL}} P_\Phi(k_1) P_\Phi(k_2) + 2\ \text{perm.}, \tag{2}$$

with the curvature power spectrum $P_\Phi(k)$ defined in terms of the Gaussian component alone as $\langle\phi(\boldsymbol{k}_1)\phi(\boldsymbol{k}_2)\rangle = \delta_{\mathrm{D}}^{(3)}(\boldsymbol{k}_{12}) P_\Phi(k_1)$, where we introduce the notation $\boldsymbol{k}_{ij} \equiv \boldsymbol{k}_i + \boldsymbol{k}_j$. The magnitude of the curvature bispectrum is maximized for the 'squeezed' triangular configuration, i.e. when one side of the triangle is much smaller than the other two, say $k_1 \ll k_2 \simeq k_3$. The curvature trispectrum is given by

$$T_\Phi(\boldsymbol{k}_1, \boldsymbol{k}_2, \boldsymbol{k}_3, \boldsymbol{k}_4) = 4 f_{\mathrm{NL}}^2 P_\Phi(k_1) P_\Phi(k_2) \times [P_\Phi(k_{13}) + P_\Phi(k_{14})] + 5\ \text{perm.} \tag{3}$$

The linear matter overdensity in Fourier space $\delta_{\boldsymbol{k}}$ is related to the curvature perturbations $\Phi_{\boldsymbol{k}}$ via the Poisson equation

$$\delta_{\boldsymbol{k}}(z) = M(k, z)\, \Phi_{\boldsymbol{k}}, \tag{4}$$

where we introduced the function

$$M(k, z) = \frac{2}{3} \frac{k^2 T(k) D(z)}{\Omega_{\mathrm{m}} H_0^2}, \tag{5}$$

with $T(k)$ being the matter transfer function, computed with the CAMB code (Lewis, Challinor & Lasenby 2000), and $D(z)$ the growth factor in units of $1 + z$. The initial matter correlators are related to the correlators of the curvature perturbations through

$$\langle\delta_{\boldsymbol{k}_1} \cdots \delta_{\boldsymbol{k}_n}\rangle = M(k_1, z) \cdots M(k_n, z) \langle\Phi_{\boldsymbol{k}_1} \cdots \Phi_{\boldsymbol{k}_n}\rangle, \tag{6}$$

© 2010 The Authors. Journal compilation © 2010 RAS, MNRAS **406,** 1014–1028

so that the linear power spectrum is given by

$$P_0(k) = M^2(k, z)P_\Phi(k), \tag{7}$$

while the initial bispectrum and trispectrum are, respectively, given by

$$B_0(k_1, k_2, k_3) = M(k_1)M(k_2)M(k_3)B_\Phi(k_1, k_2, k_3) \tag{8}$$

and

$$T_0(\boldsymbol{k}_1, \boldsymbol{k}_2, \boldsymbol{k}_3, \boldsymbol{k}_4) = M(k_1)M(k_2)M(k_3)M(k_4) \times T_\Phi(\boldsymbol{k}_1, \boldsymbol{k}_2, \boldsymbol{k}_3, \boldsymbol{k}_4)\,. \tag{9}$$

As we will see shortly, non-linear corrections to the matter bispectrum will depend on both the initial bispectrum B_0 *and* trispectrum T_0.

2.2 Perturbation theory

In PT, the solution for the non-linear matter density contrast $\delta_{\boldsymbol{k}}$ in Fourier space is given in terms of corrections to the linear solution $\delta^{(1)}$ (Fry 1984), so that

$$\delta_{\boldsymbol{k}} = \delta^{(1)}_{\boldsymbol{k}} + \delta^{(2)}_{\boldsymbol{k}} + \delta^{(3)}_{\boldsymbol{k}} + \cdots, \tag{10}$$

where each non-linear correction is given by

$$\delta^{(n)}_{\boldsymbol{k}} \equiv \int \mathrm{d}^3q_1 \ldots \mathrm{d}^3q_n\, F_n(\boldsymbol{q}_1, \ldots, \boldsymbol{q}_n)\, \delta^{(1)}_{\boldsymbol{q}_1} \ldots \delta^{(1)}_{\boldsymbol{q}_n}, \tag{11}$$

with $F_n(\boldsymbol{q}_1, \ldots, \boldsymbol{q}_n)$ being the *symmetrized* kernel of the n-order solution. Equation (10) allows one to derive the evolved matter correlators once the initial correlators, i.e. the correlators of the linear $\delta^{(1)}_{\boldsymbol{k}}$, are known. For Gaussian initial conditions, only the linear power spectrum P_0 must be specified. In general, however, higher order correlators need to be taken into account.

In analogy with quantum field theory, perturbative solutions for the matter correlators can be denoted as *tree-level*, *one-loop*, *two-loop*, etc., according to the number of internal integrations present in their expressions. However, it should be noted that while in the case of Gaussian initial conditions the number of loops of the perturbative correction correspond univocally to a specific perturbative order, this is, as we will see below, no longer true for non-Gaussian initial conditions.

For completeness, we summarize here the explicit expressions of the one-loop PT expansion for both the matter power spectrum and the bispectrum with generic non-Gaussian initial conditions. In the case of the matter power spectrum, we have up to fourth order in PT (see Bernardeau et al. 2002, and reference therein)

$$P(k) = P_{11}(k) + P_{12}(k) + P^I_{22} + P^I_{13} + \text{two-loop terms} + \mathcal{O}\left(\delta_0^5\right), \tag{12}$$

where $P_{11} \equiv P_0$ is the linear matter power spectrum, while

$$P_{12} = 2\int \mathrm{d}^3q\, F_2(\boldsymbol{q}, \boldsymbol{k}-\boldsymbol{q})\; B_0(k, q, |\boldsymbol{k}-\boldsymbol{q}|), \tag{13}$$

$$P^I_{22} = 2\int \mathrm{d}^3q\, F_2^2(\boldsymbol{q}, \boldsymbol{k}-\boldsymbol{q})\; P_0(q)\; P_0(|\boldsymbol{k}-\boldsymbol{q}|), \tag{14}$$

$$P^I_{13} = 6\; P_0(k) \int \mathrm{d}^3q\, F_3(\boldsymbol{k}, \boldsymbol{q}, -\boldsymbol{q})\; P_0(q). \tag{15}$$

We can see that the only additional contribution due to primordial non-Gaussianity is $P_{12}(k)$ which depends on the initial bispectrum B_0 (neglecting two-loop contributions at the fourth order in PT that depend on the initial trispectrum). The amplitude of this correction for local non-Gaussian initial conditions was studied in Taruya et al. (2008), who also considered initial conditions of the equilateral kind. They found that the effect of a primordial non-Gaussian component within the bounds from CMB observations is typically below 1 per cent at mildly non-linear scales, at the limit of detectability in future large-scale structure observations.

One-loop corrections to the matter bispectrum for Gaussian initial conditions have been studied in Scoccimarro (1997) and Scoccimarro et al. (1998), while the extension to generic non-Gaussian initial conditions is explored in Sefusatti (2009). For the bispectrum up to sixth order in PT and excluding two-loop corrections, we have the following expression:

$$B = B_{111} + B^I_{112} + B^{II}_{112} + B^I_{122} + B^{II}_{122} + B^I_{113} + B^{II}_{113} + B^I_{222} + B^I_{123} + B^{II}_{123} + B^I_{114} + \text{two-loop terms}, \tag{16}$$

where $B_{111} \equiv B_0$ is the initial bispectrum and

$$B^I_{112} = 2F_2(\boldsymbol{k}_1, \boldsymbol{k}_2)\; P_0(k_1)\; P_0(k_2) + 2\ \text{perm.}, \tag{17}$$

is the other tree-level contribution, while the one-loop corrections are given by

$$B^{II}_{112} = \int \mathrm{d}^3q\, F_2(\boldsymbol{q}, \boldsymbol{k}_3 - \boldsymbol{q})\; T_0(\boldsymbol{k}_1, \boldsymbol{k}_2, \boldsymbol{q}, \boldsymbol{k}_3 - \boldsymbol{q}), \tag{18}$$

$$\begin{aligned} B^I_{122} &= 2P_0(k_1)\left[F_2(\boldsymbol{k}_1, \boldsymbol{k}_3)\int \mathrm{d}^3q\, F_2(\boldsymbol{q}, \boldsymbol{k}_3 - \boldsymbol{q}) \times B_0(k_3, q, |\boldsymbol{k}_3 - \boldsymbol{q}|) + (k_3 \leftrightarrow k_2)\right] + 2\ \text{perm.}, \\ &= F_2(\boldsymbol{k}_1, \boldsymbol{k}_2)\,[P_0(k_1)\; P_{12}(k_2) + P_0(k_2)\; P_{12}(k_1)] + 2\ \text{perm.}, \end{aligned} \tag{19}$$

$$B^{II}_{122} = 4\int \mathrm{d}^3q\, F_2(\boldsymbol{q}, \boldsymbol{k}_2 - \boldsymbol{q})F_2(\boldsymbol{k}_1 + \boldsymbol{q}, \boldsymbol{k}_2 - \boldsymbol{q}) \times B_0(k_1, q, |\boldsymbol{k}_1 + \boldsymbol{q}|)\; P_0(|\boldsymbol{k}_2 - \boldsymbol{q}|) + 2\ \text{perm.}, \tag{20}$$

$$B^I_{113} = 3B_0(k_1, k_2, k_3)\int \mathrm{d}^3q\, F_3(\boldsymbol{k}_3, \boldsymbol{q}, -\boldsymbol{q})P_0(q) + 2\ \text{perm.}, \tag{21}$$

$$B^{II}_{113} = 3P_0(k_1)\int \mathrm{d}^3q\, F_3(\boldsymbol{k}_1, \boldsymbol{q}, \boldsymbol{k}_2 - \boldsymbol{q})B_0(k_2, q, |\boldsymbol{k}_2 - \boldsymbol{q}|) + (k_1 \leftrightarrow k_2) + 2\ \text{perm.}, \tag{22}$$

$$B^I_{222} = 8\int \mathrm{d}^3q\, F_2(-\boldsymbol{q}, \boldsymbol{q} + \boldsymbol{k}_1)F_2(-\boldsymbol{q} - \boldsymbol{k}_1, \boldsymbol{q} - \boldsymbol{k}_2) \times F_2(\boldsymbol{k}_2 - \boldsymbol{q}, \boldsymbol{q})P_0(q)P_0(|\boldsymbol{k}_1 + \boldsymbol{q}|)P_0(|\boldsymbol{k}_2 - \boldsymbol{q}|), \tag{23}$$

$$B^I_{123} = 6P_0(k_1)\int \mathrm{d}^3q\, F_3(\boldsymbol{k}_1, \boldsymbol{k}_2 - \boldsymbol{q}, \boldsymbol{q})F_2(\boldsymbol{k}_2 - \boldsymbol{q}, \boldsymbol{q}) \times P_0(|\boldsymbol{k}_2 - \boldsymbol{q}|)\; P_0(q) + 5\ \text{perm.}, \tag{24}$$

$$\begin{aligned} B^{II}_{123} &= 6P_0(k_1)\; P_0(k_2)F_2(\boldsymbol{k}_1, \boldsymbol{k}_2) \times \int \mathrm{d}^3q\, F_3(\boldsymbol{k}_1, \boldsymbol{q}, -\boldsymbol{q})\; P_0(q) + 5\ \text{perm.} \\ &= F_2(\boldsymbol{k}_1, \boldsymbol{k}_2)\,[P_0(k_1)\; P_{13}(k_2) + P_0(k_2)\; P_{13}(k_1)] + 2\ \text{perm.}, \end{aligned} \tag{25}$$

$$B^{I}_{114} = 12 P_0(k_1)\, P_0(k_2) \int \mathrm{d}^3q\; F_4(\boldsymbol{q}, -\boldsymbol{q}, -\boldsymbol{k}_1, -\boldsymbol{k}_2)\, P_0(q) + 2\ \text{perm.} \tag{26}$$

Specifically, the one-loop contributions present because of non-Gaussian initial conditions are B^{II}_{112}, which depend on the initial trispectrum T_0, and all the fifth-order terms B^{I}_{122}, B^{II}_{122}, B^{I}_{113} and B^{II}_{113}, which depend on the initial bispectrum B_0.

The remaining terms, corresponding to Gaussian initial conditions, were recently studied in the context of resummation techniques of the PT series and can be regarded as perturbative expansions of 'resummed' kernels (Bernardeau, Crocce & Scoccimarro 2008). For instance, B^{II}_{123} corresponds to the next-to-leading term in the resummation of the non-linear propagator in language of Crocce & Scoccimarro (2006a,b) or $\Gamma^{(1)}$ in the notation of Bernardeau et al. (2008). That is, B^{II}_{123} can be obtained from the tree-level expression in equation (17) by replacing the linear growth D^2_+ implicit in P_0 as $D^2_+ \to \mathrm{D}^2_+(1 + \mathrm{P}_{13}/P_0)$. Similarly, B^{I}_{114} corresponds to a redefinition (or resummation) of the F_2 kernel. In turn, B^{I}_{123} and B^{I}_{222} are leading terms whose corrections appear at higher order in the PT series of equation (16). The resummed kernels have well-defined properties in terms of tree-level quantities and might be the window to an accurate description of the non-linear bispectrum at non-linear scales.

In Fig. 1 we show the different components in PT to the equilateral configurations (upper panels) and to the squeezed configurations (lower panels) of the matter bispectrum: $B(k, k, k)$ and $B(k, k, \Delta k)$, respectively, with $\Delta k \simeq 0.012\, h\,\mathrm{Mpc}^{-1}$ as a function of k. In the left-hand panels, we compare the tree-level contributions B_{111} with $f_{\rm NL} = 100$ (short-dashed, red lines) and B^{I}_{112} (long-dashed, blue lines) to the sum of the one-loop corrections $B_{222} + B^{I}_{123} + B^{II}_{123} + B_{114}$ (dot–dashed, blue lines) present for Gaussian initial conditions and to the sum of the one-loop corrections due to primordial non-Gaussianity, $B^{II}_{112} + B^{I}_{122} + B^{II}_{122} + B^{I}_{113} + B^{II}_{113}$, with $f_{\rm NL} = 100$ (dotted, red lines). The central and right-hand panels compare these sums of one-loop corrections to their individual contributions. For the 'Gaussian' piece (central panels), note that we plot $-B^{II}_{123}$ and $-B_{114}$, implying that the overall one-loop correction is the result of a number of cancellations similar to those occurring for the one-loop corrections to the matter power spectrum. Analogous considerations also apply to the 'non-Gaussian' one-loop corrections (right-hand panels), where such cancellations strongly depend on the triangular configuration.

To conclude the section, we note that the 'order' of each correction in the perturbative expansion is defined in terms of the power of the linear *matter* density field, $\delta^{(1)}$. An alternative convention could be given by counting the powers of the Gaussian contribution to the curvature perturbations, that is ϕ in equation (1). Our choice is motivated by the standard use in the large-scale structure literature and by the fact that to the nth perturbative order corresponds the well-defined redshift dependence $D^n(z)$. On the other hand, we can keep track of the expansion in ϕ in terms of the non-linear parameter $f_{\rm NL}$.

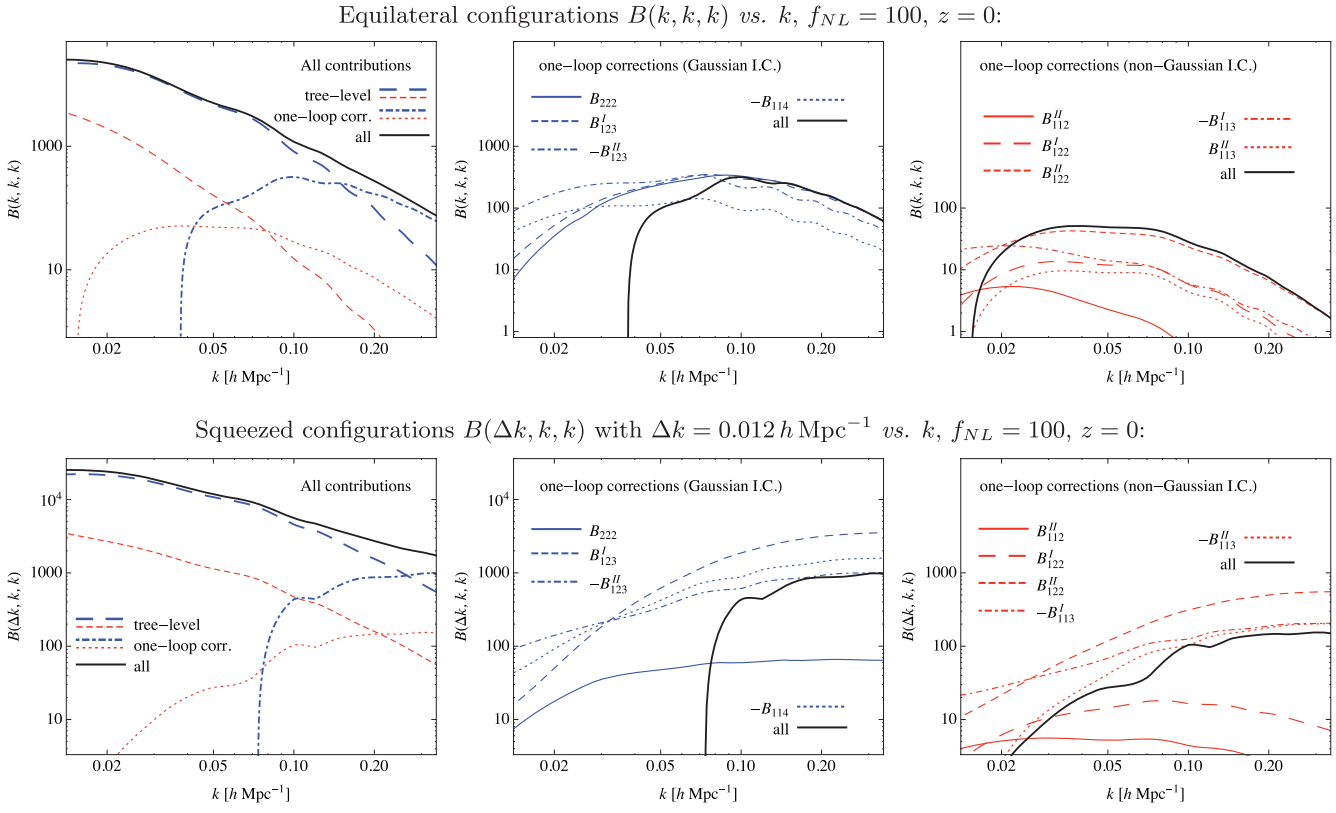

Figure 1. Different components to the PT one-loop prediction for the equilateral configurations $B(k, k, k)$ (upper panel) and the squeezed configurations $B(\Delta k, k, k)$ with $\Delta k \simeq 0.01\, h\,\mathrm{Mpc}^{-1}$ (lower panels) of the matter bispectrum. The left-hand panels show the full prediction at one loop assuming $f_{\rm NL} = 100$ (black, continuous line), together with the tree-level components B_{111} (short dashed, red) and B^{I}_{112} (long-dashed, blue) and the one-loop corrections present for Gaussian initial conditions (dot–dashed, blue) and those depending instead on the initial bispectrum and trispectrum (dotted, red). The central panels show the individual terms of the one-loop corrections for Gaussian initial conditions, while the right-hand panels show the individual components of the one-loop corrections present only for non-Gaussian initial conditions.

© 2010 The Authors. Journal compilation © 2010 RAS, MNRAS **406,** 1014–1028

3 SIMULATIONS

We utilize a series of large 1024^3 N-body simulations of the Λ cold dark matter cosmology seeded with Gaussian and non-Gaussian initial conditions (Desjacques et al. 2009). The box size is $1600\,h^{-1}$ Mpc with a force resolution of 0.04 times the mean inter-particle distance. The (dimensionless) power spectrum of the Gaussian part $\phi(\boldsymbol{x})$ of the Bardeen potential is the usual power law $\Delta^2_\phi(k) \equiv k^3 P_\phi(k)/(2\pi^2) = A_\phi (k/k_0)^{n_s-1}$. The non-Gaussianity is of the local form described above. We adopt the standard (CMB) convention in which $\phi(\boldsymbol{x})$ is primordial and not extrapolated to the present epoch. We assume $h = 0.7, \Omega_m = 0.279, \Omega_b = 0.0462, n_s = 0.96$ and a normalization of the Gaussian curvature perturbations $A_\phi = 7.96 \times 10^{-10}$ at the pivot point $k_0 = 0.02\,\mathrm{Mpc}^{-1}$, close to the best-fitting values inferred from CMB measurements (Komatsu et al. 2009b). This yields a density fluctuation amplitude $\sigma_8 \simeq 0.81$ when the initial conditions are Gaussian. Eight sets of three simulations, each of which has $f_{NL} = 0, \pm 100$, were run with the N-body code SHAPE GADGET (Springel 2005). The same Gaussian random seed field ϕ is employed in each set of runs so as to minimize the sampling variance. The initial particle distribution is generated at redshift $z_i = 99$ using the Zel'dovich approximation (Zel'Dovich 1970).

3.1 Bispectrum estimator and triangle bins

Let us now introduce the bispectrum estimator $\hat{B}(k_1, k_2, k_3)$ used in the analysis of the N-body simulations. For a cubic box of volume V, this is given by (Scoccimarro et al. 1998)

$$\hat{B} \equiv \frac{V_f}{V_B} \int_{k_1} \mathrm{d}^3 q_1 \int_{k_2} \mathrm{d}^3 q_2 \int_{k_3} \mathrm{d}^3 q_3\, \delta_D(\boldsymbol{q}_{123})\, \delta_{\boldsymbol{q}_1}\, \delta_{\boldsymbol{q}_2}\, \delta_{\boldsymbol{q}_3}, \tag{27}$$

where $V_f \equiv k_f^3 = (2\pi)^3/V$ is the volume of the fundamental cell and where each integration is defined over the bin $q_i \in [k_i - \Delta k/2, k_i + \Delta k/2]$ centred at k_i and of size Δk equal to a multiple of the fundamental frequency k_f. In our case, we assume a bin size $\Delta k = 3k_f$. The Dirac delta function $\delta_D(\boldsymbol{q}_{123})$ ensures that the wavenumbers $\boldsymbol{q}_1, \boldsymbol{q}_2$ and $\boldsymbol{q}_3$ indeed form a closed triangle, as imposed by translational invariance. The normalization factor $V_B(k_1, k_2, k_3)$ given by

$$V_B(k_1, k_2, k_3) \equiv \int_{k_1} \mathrm{d}^3 q_1 \int_{k_2} \mathrm{d}^3 q_2 \int_{k_3} \mathrm{d}^3 q_3\, \delta_D(\boldsymbol{q}_{123}) \simeq 8\pi^2\, k_1 k_2 k_3\, \Delta k^3 \tag{28}$$

represents the number of *fundamental* triangular configurations (labelled by the triplet $\boldsymbol{q}_1, \boldsymbol{q}_2$ and $\boldsymbol{q}_3$) that belong to the triangular configuration *bin* defined by the triangle sizes k_1, k_2 and k_3 with uncertainty Δk. In order to better interpret the simulation results, we provide as well the expression for the variance of the bispectrum associated with this estimator. At leading order, the variance reads as (Scoccimarro et al. 1998)

$$\Delta B^2(k_1, k_2, k_3) = s_B \frac{V_f}{V_B} P(k_1) P(k_2) P(k_3), \tag{29}$$

where the symmetry factor $s_B(k_1, k_2, k_3) = 6, 2$ or 1 for equilateral, isosceles or scalene configurations, respectively. This expression neglects further corrections depending on the matter bispectrum, trispectrum and six-point functions that are responsible for correlations between different configurations (see Sefusatti et al. 2006).

When comparing the measured bispectrum configurations to the theoretical predictions in PT, one should be careful to properly account for the effect of the finite size of the triangle bins. As explained above, each configuration is defined in terms of the sides of the triangle with k_i being the central value and Δk the uncertainty. Since we are assuming $\Delta k = 3k_f$, a typically large number of 'fundamental' triangles fall into each triangle bin. For instance, it is easy to see that in the case of equilateral configurations, the bin defined by the central value k will include equilateral triangles of side $q = k - k_f$ or $q = k + k_f$ just as well as nearly equilateral triangles with different sides still belonging to the k-bin. What is important here is the fact that in the case of equilateral configurations, we will have slightly *more* triangles of a size larger than the fundamental equilateral triangle with side $q = k$ than triangles of a smaller size. This simply follows from the larger number of modes at larger q.

The correct approach consists in computing the raw PT prediction $B^{PT}(q_1, q_2, q_3)$ *and average it over the triangle bin* defined by k_1, k_2, k_3 and Δk, that is

$$B^{th}(k_1, k_2, k_3) = \frac{1}{V_B} \int_{k_1} \mathrm{d}^3 q_1 \int_{k_2} \mathrm{d}^3 q_2 \int_{k_3} \mathrm{d}^3 q_3\, \delta_D(\boldsymbol{q}_{123}) \times B^{PT}(q_1, q_2, q_3), \tag{30}$$

where B^{th} is the value to be compared with the measurements. This is, however, computationally challenging especially in the case of the one-loop corrections to the bispectrum, which usually involve three-dimensional integrations. An alternative solution, less rigorous yet reasonable given the uncertainties of our measurements, consists in defining the following *effective* values $\tilde{k}_i$ for the wavenumbers k_i characterizing the triangle:

$$\tilde{k}_i = \frac{1}{V_B} \int_{k_1} \mathrm{d}^3 q_1 \int_{k_2} \mathrm{d}^3 q_2 \int_{k_3} \mathrm{d}^3 q_3\, \delta_D(\boldsymbol{q}_{123})\, q_i, \tag{31}$$

so that the theoretical prediction which the binned measurements of the bispectrum must be compared to is

$$B^{th}(k_1, k_2, k_3) = B^{PT}(\tilde{k}_1, \tilde{k}_2, \tilde{k}_3). \tag{32}$$

This procedure improves significantly the agreement between theory and simulations, particularly for 'squeezed' configurations where $k_1 \ll k_2 \simeq k_3$.

Here and henceforth, all theoretical predictions will be computed in terms of the effective triangle $\tilde{k}_1$, $\tilde{k}_2$ and $\tilde{k}_3$ as defined above. Furthermore, when the bispectrum is expressed as a function of the angle θ between two of the three wavemodes, it is convenient to introduce an *effective* angle $\tilde{\theta}$ given by

$$\cos\tilde{\theta}(k_1, k_2; k_3) = \frac{1}{V_B} \int_{k_1} \mathrm{d}^3 q_1 \int_{k_2} \mathrm{d}^3 q_2 \int_{k_3} \mathrm{d}^3 q_3\, \delta_D(\boldsymbol{q}_{123}) \times \cos\theta(q_1, q_2; q_3), \tag{33}$$

where $\theta(q_1, q_2; q_3)$ is the angle between the vectors $\boldsymbol{q}_1$ and $\boldsymbol{q}_2$. This expression defines the effective angle as a weighted average of the angles corresponding to the 'fundamental' triangles falling in a given bin. These are limited by the triangle inequalities $q_3 \leq q_1 + q_2$ and $q_3 \geq |q_1 - q_2|$. In the figures, the quantities measured in the N-body simulations will be plotted as a function of $\tilde{\theta}$, while the theoretical expectations will be the raw PT predictions.

3.2 The power spectrum

To facilitate the comparison between different statistics and help interpreting the bispectrum measurements of the next section, we will first present measurements of the matter power spectrum, highlighting the effects due to primordial non-Gaussianity and their description in PT. Similar results can be found in Desjacques et al. (2009), Grossi et al. (2008), Pillepich et al. (2010) and Bartolo et al. (2009).

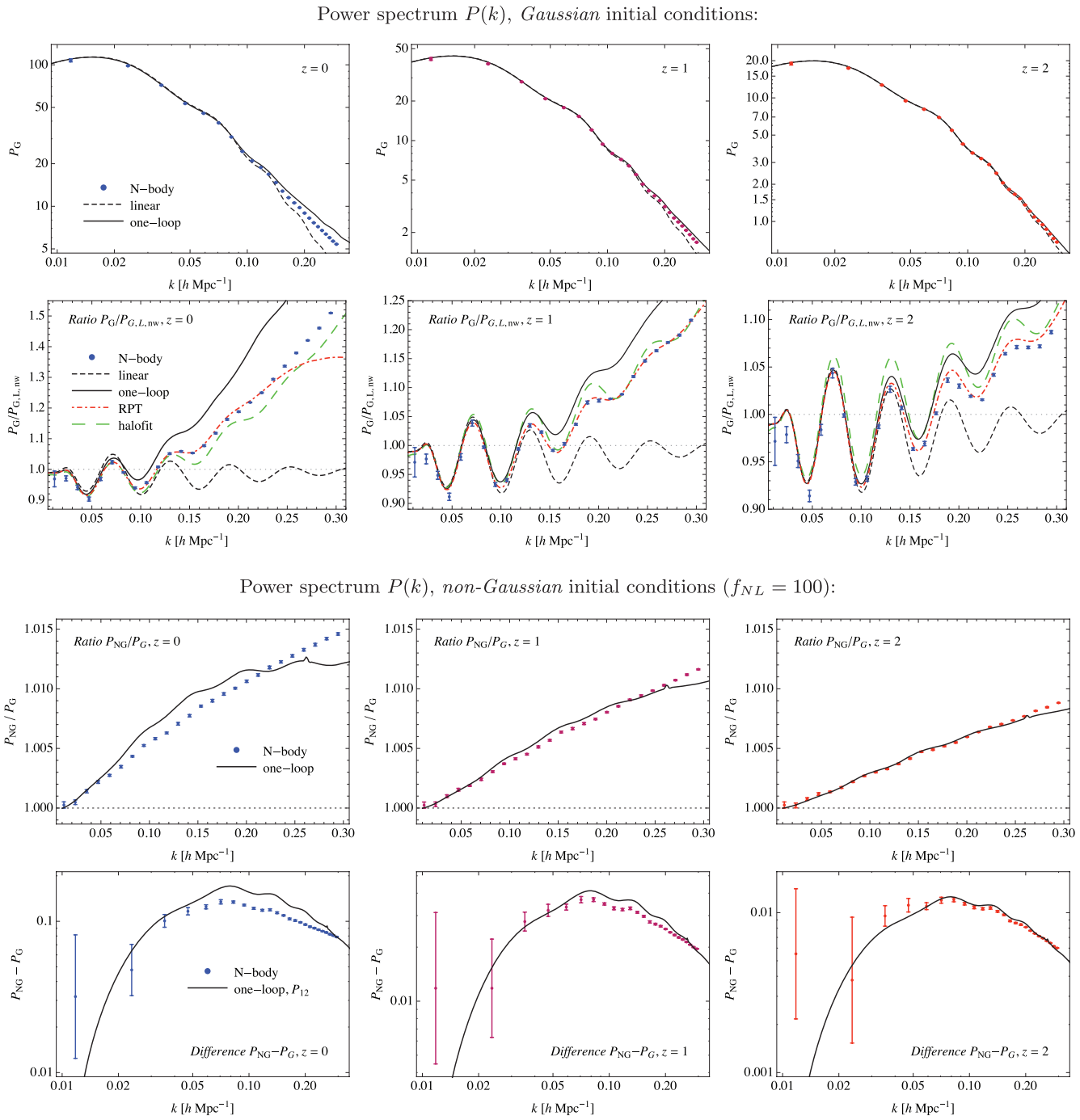

Figure 2. Measurements of the matter power spectrum, $P(k)$, as a function of k. We show, from top to bottom, the power spectrum B (first row) and its ratio to the no-wiggle, linear prediction (second row) for Gaussian initial conditions, the ratio $P(f_{\rm NL} = +100)/P(f_{\rm NL} = 0)$ (third row) and the difference $P(f_{\rm NL} = +100) - P(f_{\rm NL} = 0)$ (last row). Different columns correspond to redshifts $z = 0, 1$ and 2. The short-dashed, black line indicates the tree-level PT predictions while continuous, black lines the one-loop ones. In addition, on the second row we include the RPT prediction of Crocce & Scoccimarro (2006a) (at the two-loop approximation, dot–dashed, red line) and the prediction from the code HALOFIT of Smith et al. (2003) (long-dashed, green line).

In the upper two rows of Fig. 2, we show the matter power spectrum measured in simulations of Gaussian initial conditions as well as the linear (dashed lines) and one-loop (continuous lines) predictions in PT. In addition, in the second row, displaying the ratio of the Gaussian power spectrum to a smooth (i.e. no-wiggles) linear power spectrum, we show the non-linear power spectrum obtained with the HALOFIT code of Smith et al. (2003) (thin, green line) and the predictions in renormalized PT (RPT; Crocce & Scoccimarro 2006a,b 2008). The various columns correspond, from left to right, to the redshifts $z = 0$, 1 and 2, respectively. The well-known failure of one-loop PT to describe the matter power spectrum at mildly non-linear scales and low redshift is quite apparent [see Crocce & Scoccimarro (2008) and Jeong & Komatsu (2006) for a recent comparison with simulations and for a comparison at high redshift, respectively]. The HALOFIT prediction is significantly better at low redshift, while it shows a discrepancy of the same order at $z = 2$.

© 2010 The Authors. Journal compilation © 2010 RAS, MNRAS **406,** 1014–1028

On the other hand, the RPT prescription provides very good predictions (within 1 per cent) up to $0.23\,h\,\mathrm{Mpc}^{-1}$ at redshift zero and over the whole range we consider at redshifts $z = 1$ and 2. The slight discrepancy at $z = 2$, of the order of 0.5 per cent, not present at $z = 1$, might perhaps be explained in terms of transients from the initial conditions (Scoccimarro 1998; Crocce, Pueblas & Scoccimarro 2006), despite the relatively high redshift ($z = 99$) assumed for the simulations.

In the third row, we show the ratio of the matter power spectrum extracted from $f_{\rm NL} = 100$ to Gaussian simulations. The plots for $z = 0$ and $z = 2$ reproduce fig. 3 in Desjacques et al. (2009). Finally, the last row shows the *difference* between the two cases, i.e. $P(k; f_{\rm NL} = 100) - P(k; f_{\rm NL} = 0)$. In all these plots, the ratio and the difference measured in the simulations are computed for each realization and then averaged over the eight realizations available. At redshift zero, the one-loop correction P_{12} reproduces qualitatively the effect due to primordial non-Gaussianity, but it breaks down at relatively large scales, $k \sim 0.2\,h\,\mathrm{Mpc}^{-1}$, maybe suggesting the need for higher order corrections. An extension of PT such as the time-renormalization group approach (Matarrese & Pietroni 2007; Pietroni 2008) seems to improve only in part the agreement between theory and simulations beyond this scale (see fig. 4 in Bartolo et al. 2009).

In each realization of the initial conditions with $f_{\rm NL} = 0, \pm 100$, we also measured the combination $[P(k; f_{\rm NL} = +100) + P(k; f_{\rm NL} = -100) - 2P(k; f_{\rm NL} = 0)]/2$. In the PT framework, the result is expected to be the sum of all the corrections depending on even powers of $f_{\rm NL}$. At the lowest order, however, these are given by two-loop contributions which we ignore in this work. Nevertheless, we find that in the range of scale considered here and for $f_{\rm NL} = 100$, such terms represent an effect of the order of 10^{-4} relative to the power spectrum for Gaussian initial conditions.

4 RESULTS

We now present the measurements of the matter bispectrum with Gaussian and non-Gaussian initial conditions together with one-loop PT predictions. In the figures, we will often denote these quantities as $B_{\rm G}$ and $B_{\rm NG}$, where the 'G' and 'NG' subscripts refer to the initial conditions. In the Gaussian case moreover, we will also perform a comparison between the measurements and the fitting formula of Scoccimarro & Couchman (2001).

To assess the agreement between PT and N-body measurements as a function of scale and triangle shape, we will consider five sets of configurations. We will present results as a function of k for equilateral configurations $B(k, k, k)$, isosceles configurations $B(2k, 2k, k)$ as well as increasingly 'squeezed' configurations $B(k, k, \Delta k)$ with fixed Δk. To further explore the shape dependence, we will also show the result of measuring the matter bispectrum for two sets of generic configurations for which the magnitude of two sides of the triangle (k_1 and k_2) is fixed while the angle θ between them is varied.

For each of these sets, in Figs 3 to 7 the upper two panels show measurements of the matter bispectrum B, or the *reduced* bispectrum Q (see equation 34), for *Gaussian* initial conditions, as well as the ratio to the corresponding tree-level expression in PT where the acoustic oscillations are removed by means of the smooth transfer function of Eisenstein & Hu (1998). Recall that there is no 'linear' matter bispectrum for Gaussian initial conditions (but there is an initial bispectrum in the presence of primordial non-Gaussianity). For the sake of comparison, we take the tree-level prediction as a reference since it is most directly related to the linear bispectrum, which is generically $B^{\rm tree} \sim P_{\rm L}^2$.

The last three rows in the plots focus on the effect of primordial non-Gaussianity. We show, in particular, the ratio

$$B(f_{\rm NL} = 100)/B(f_{\rm NL} = 0) \quad \text{(third row)},$$

the difference

$$B(f_{\rm NL} = 100) - B(f_{\rm NL} = 0) \quad \text{(fourth row)},$$

with respect to the Gaussian case, and the combination

$$[B(f_{\rm NL} = +100) + B(f_{\rm NL} = -100) - 2B(f_{\rm NL} = 0)]/2 \quad \text{(last row)}$$

to highlight the effects proportional to $f_{\rm NL}^2$. In all cases, the N-body results indicate the mean over eight realizations of the specific combination (ratio, difference, etc.) performed with Gaussian and non-Gaussian initial conditions drawn from the same random seed field ϕ (see Section 3). In this way, we can study the effect of non-Gaussianity without the additional sampling variance affecting, for instance, the difference $B_{\rm NG} - B_{\rm G}$ obtained as the *difference* between the *mean* $B_{\rm NG}$ and the *mean* $B_{\rm G}$ over the eight realizations. Finally, the three columns correspond to the results at redshifts $z = 0$, 1 and 2. In all the plots, the numerical results are compared to the tree-level (short-dashed, black lines) and one-loop predictions (continuous, black lines) in PT.

In Fig. 3, we show the matter bispectrum $B(k, k, k)$ for equilateral configurations. As can be seen, non-linearities are particularly severe, consisting in an almost $\sim$300 per cent correction relative to the tree-level prediction for $k \simeq 0.2\,h\,\mathrm{Mpc}^{-1}$ and $z = 0$ for instance. The bispectrum measured from a total simulation volume of $\sim 33\,h^{-3}\,\mathrm{Gpc}^3$ presents errors of the order of 10 per cent at this scale for equilateral configurations. Note that this specific triangle shape suffers, unlike other configurations close in shape and scale, from a relatively large variance (up to a factor of 6). This effect originates partly from the symmetry factor s_B in equation (29) and from the large contribution of higher order correlation functions to the bispectrum variance.

The one-loop prediction appears to be well within our errors up to $k \sim 0.15\,h\,\mathrm{Mpc}^{-1}$ and describes reasonably well the behaviour at smaller scales. For $k \lesssim 0.15\,h\,\mathrm{Mpc}^{-1}$, the one-loop prediction behaves better than the fitting formula of Scoccimarro & Couchman (2001) (in the plots SC01), which under-predicts the data points at mildly non-linear scales. This $\sim$20 per cent discrepancy, unsurprising given the size of the simulation box used for the fit ($240\,h^{-1}$ Mpc), has already been noted by Pan et al. (2007). It should be remarked that the SC01 formula aimed at describing the non-linear bispectrum at smaller scales, particularly for weak lensing applications, and did not address specifically the issue of the acoustic features. Pan et al. (2007) also proposed a phenomenological model for the matter bispectrum based on a rescaling argument similar to the one explored in Hamilton et al. (1991) and Peacock & Dodds (1996). We also compared this prescription to our measurements and found that it agrees better than the fitting function of Scoccimarro & Couchman (2001). However, the rescaling induces a large and unphysical shift in the acoustic oscillations that should be properly accounted for [in Pan et al. (2007), comparisons are shown with simulations of featureless matter power spectra].

The third row of Fig. 3 shows the effect of primordial non-Gaussianity in terms of the ratio $B(f_{\rm NL} = 100)/B(f_{\rm NL} = 0)$. It is interesting to note that the additional non-linear contributions due to non-Gaussian initial conditions correspond, for these set of configurations, to an $\sim$5 per cent correction regardless of redshift. In fact, the contribution of the initial bispectrum B_0 to this effect

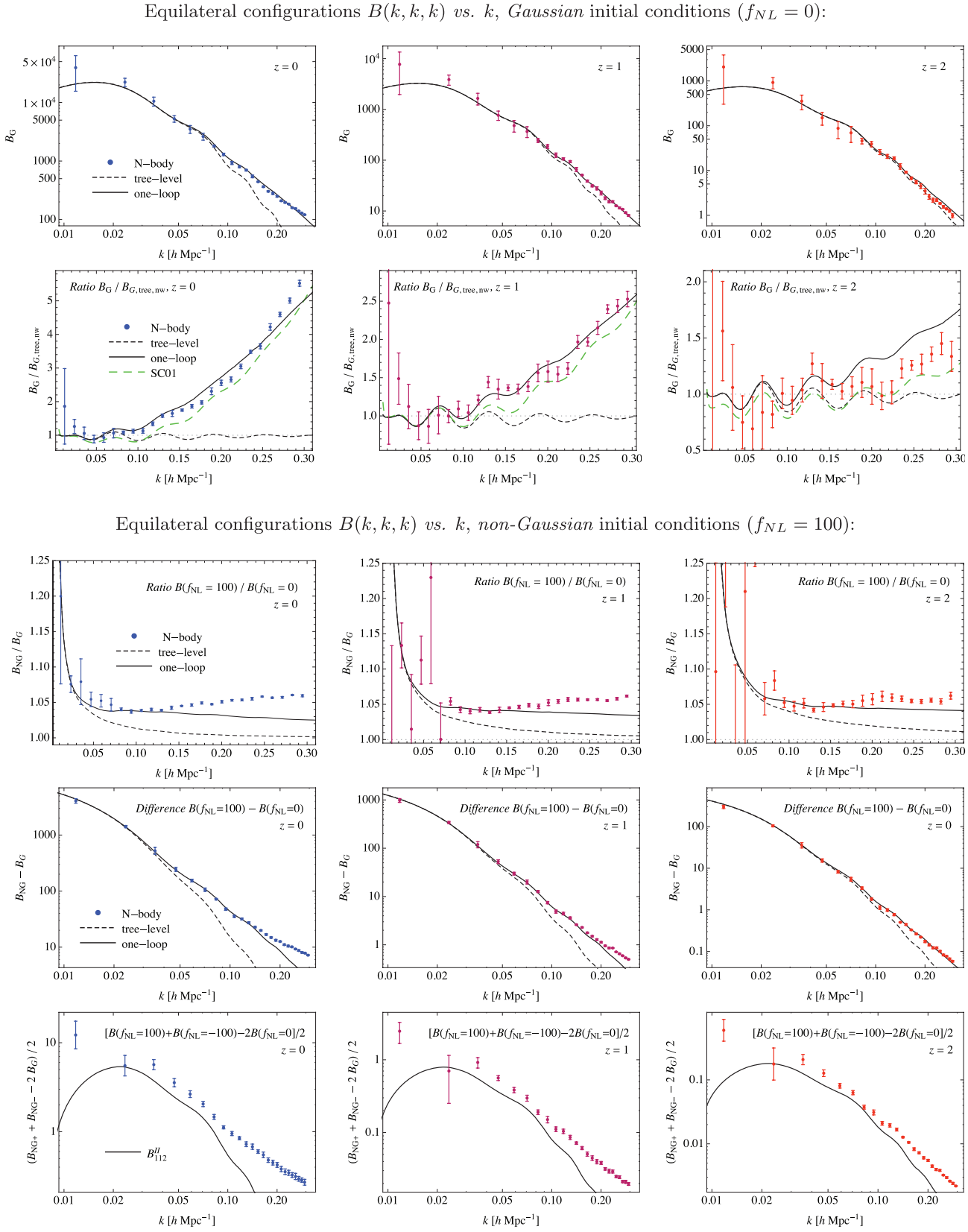

Figure 3. Measurements of the equilateral configurations of the matter bispectrum, $B(k, k, k)$, as a function of k. We show, from top to bottom, the matter bispectrum B (first row) and its ratio to the no-wiggle tree-level prediction (second row) for Gaussian initial conditions, the ratio $B(f_{\mathrm{NL}}=+100)/B(f_{\mathrm{NL}}=0)$ (third row), the difference $B(f_{\mathrm{NL}}=+100) - B(f_{\mathrm{NL}}=0)$ (fourth row) and the combination $[B(f_{\mathrm{NL}}=+100) + B(f_{\mathrm{NL}}=-100) - 2B(f_{\mathrm{NL}}=0)]/2$ (last row). Different columns correspond to redshifts $z=0$, 1 and 2. The short-dashed, black line indicate the tree-level PT predictions while continuous, black lines the one-loop ones. In addition, on the second row we include the fitting formula of Scoccimarro & Couchman (2001) (long-dashed, green lines).

© 2010 The Authors. Journal compilation © 2010 RAS, MNRAS **406,** 1014–1028

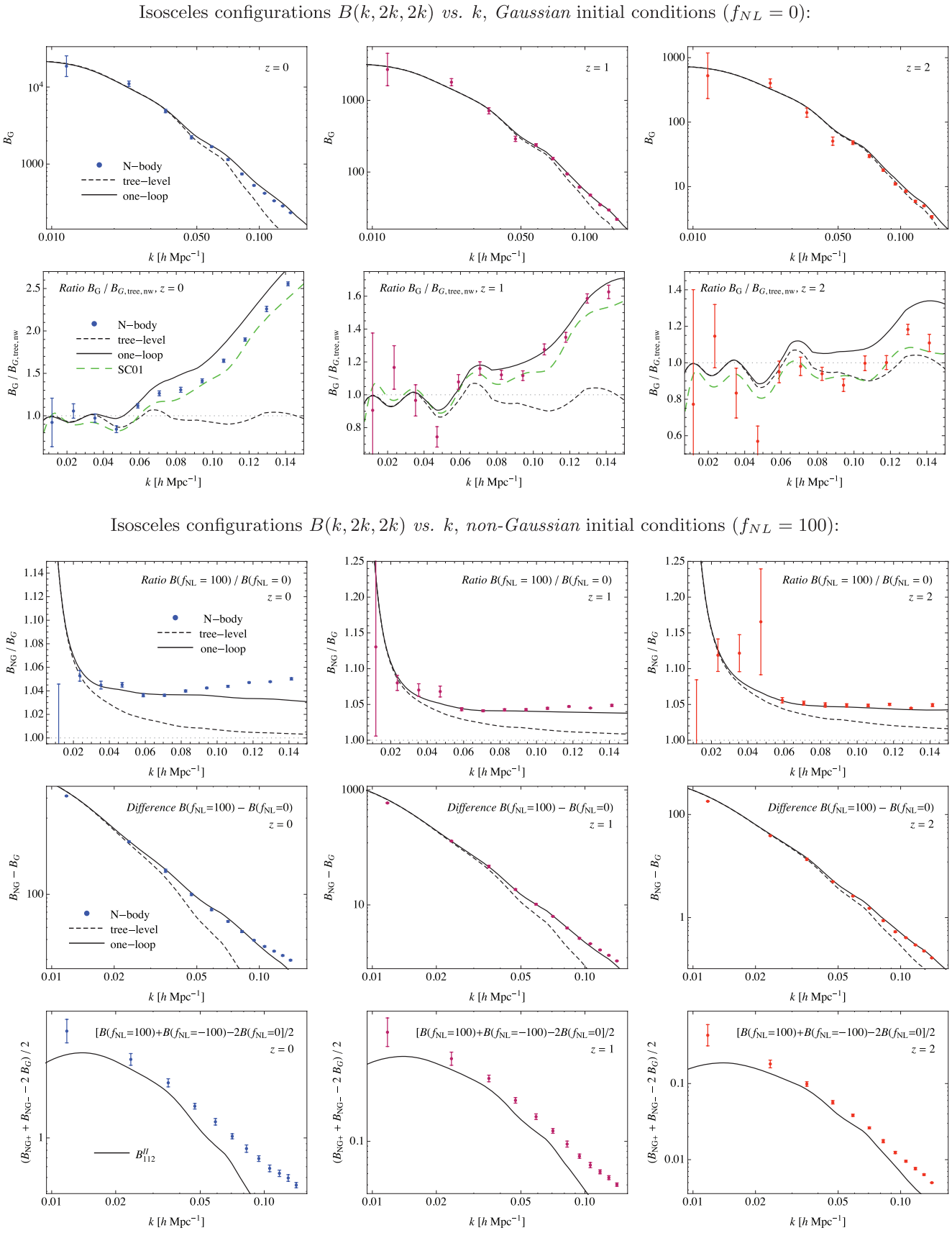

Figure 4. Same as Fig. 3, but for isosceles configurations, $B(2k, 2k, k)$, as a function of k.

© 2010 The Authors. Journal compilation © 2010 RAS, MNRAS **406,** 1014–1028

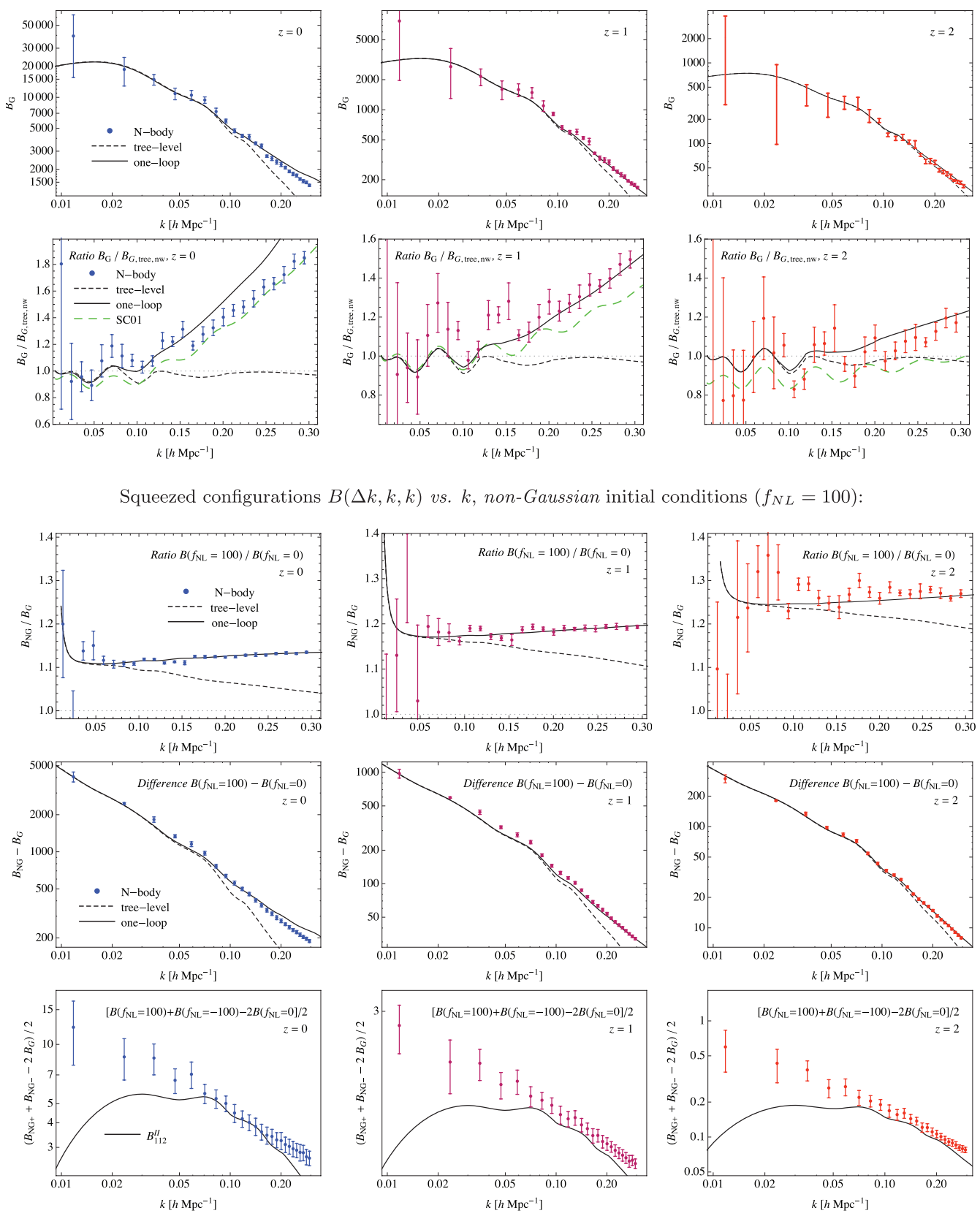

Figure 5. Same as Fig. 3, but for squeezed configurations, $B(\Delta k, k, k)$, with $\Delta k = 3k_{\mathrm{f}} \simeq 0.012\,h\,\mathrm{Mpc}^{-1}$ as a function of k.

© 2010 The Authors. Journal compilation © 2010 RAS, MNRAS **406,** 1014–1028

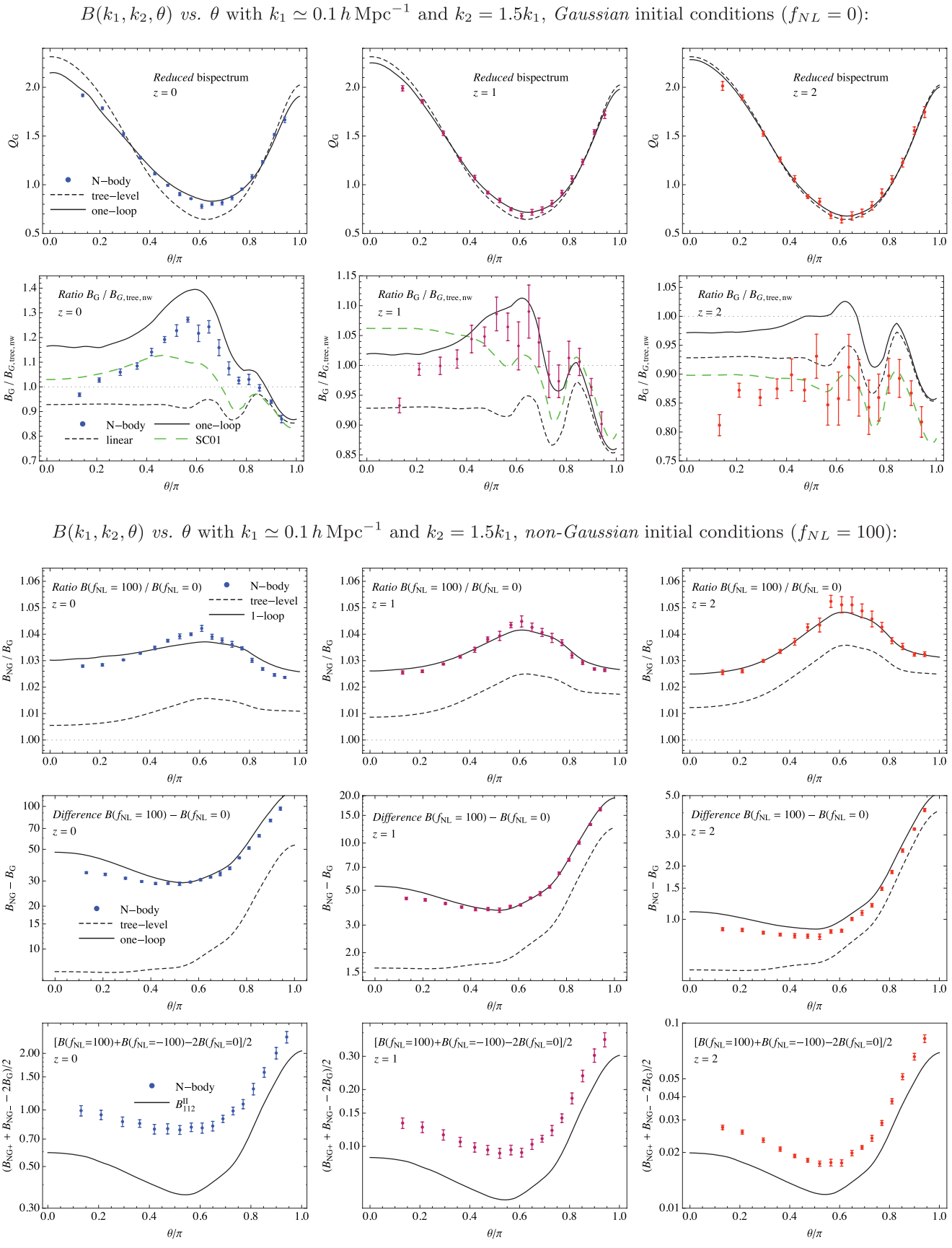

Figure 6. Same as Fig. 3 but for generic configurations $B(k_1, k_2, \theta)$ with $k_1 = 0.094\,h\,\mathrm{Mpc}^{-1}$ and $k_2 = 1.5k_1$ as a function of the angle θ between k_1 and k_2. Note that the first row now shows the *reduced* bispectrum $Q(k_1, k_2, k_3)$ (equation 34) rather than $B(k_1, k_2, k_3)$.

© 2010 The Authors. Journal compilation © 2010 RAS, MNRAS **406,** 1014–1028

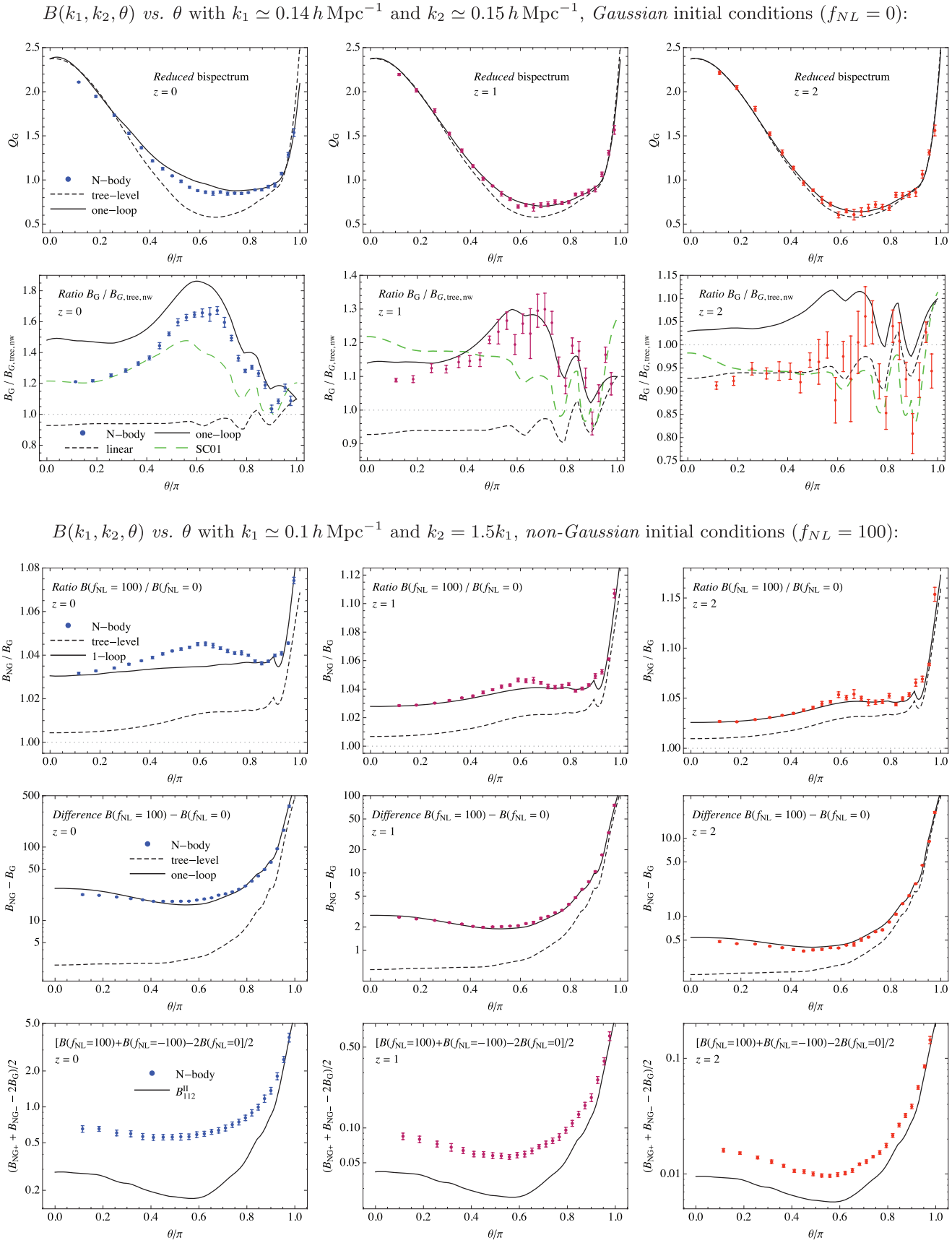

Figure 7. Same as Fig. 3 but for generic configurations $B(k_1, k_2, \theta)$ with $k_1 = 0.14\,h\,\mathrm{Mpc}^{-1}$ and $k_2 = 0.15\,h\,\mathrm{Mpc}^{-1}$ as a function of the angle θ between k_1 and k_2. Note that the first row now shows the *reduced* bispectrum $Q(k_1, k_2, k_3)$ (equation 34) rather than $B(k_1, k_2, k_3)$.

© 2010 The Authors. Journal compilation © 2010 RAS, MNRAS **406,** 1014–1028

is already subdominant at $k \sim 0.1\,h\,\mathrm{Mpc}^{-1}$ and $z = 0$, while one-loop corrections themselves fail to account for it at slightly smaller scales. This is also apparent in the difference $B(f_{\rm NL} = 100) - B(f_{\rm NL} = 0)$ which, in the PT picture, arises from the one-loop contributions depending on the initial bispectrum and trispectrum. At redshift zero, these provide an accurate description of $B(f_{\rm NL} = 100) - B(f_{\rm NL} = 0)$ up to $k \simeq 0.15\,h\,\mathrm{Mpc}^{-1}$.

Finally, in the last row we compare the combination $[B(f_{\rm NL} = +100) + B(f_{\rm NL} = -100) - 2\,B(f_{\rm NL} = 0)]/2$ to B^{II}_{112} which, in the one-loop approximation, is the sole term depending on the initial trispectrum and therefore on $f^2_{\rm NL}$. This term appears to underestimate by about 50 per cent (at best) the simulation results. One should none the less keep in mind that these contributions represent a 0.1 per cent correction to the matter bispectrum.

In Fig. 4, we show the matter bispectrum for the isosceles configurations, $B(2k, 2k, k)$, as a function of k. The shape of the triangle is unchanged while its size is rescaled. In this series of plots, the relatively smaller variance (with respect to that of the equilateral shape) expected from the above discussion is quite apparent. The error on the mean is of the order of 2–3 per cent for most of the isosceles configurations considered. These small errors allow a more accurate comparison of the measurements with PT predictions. Note that while each triangle now involves two different scales k and $2k$, the results are shown as a function of the smaller one (k) solely. For Gaussian initial conditions, the one-loop predictions systematically overestimate the data points by more than 10 per cent at $z = 0$, but the agreement substantially improves at higher redshift. By contrast, the accuracy of the fitting formula of SC01 is reasonably good for all the scales and redshifts considered. As for the effect of primordial non-Gaussianity, considerations similar to those made for equilateral configurations also hold for the isosceles shape.

In Fig. 5 we compute $B(k, k, \Delta k)$ on triangles, one side of which is held fixed to the smallest available k-bin Δk while the other two are equal and varying. k is increased smoothly such that this configuration, which represents the coupling between the scales k and Δk, asymptotes to the 'squeezed' triangle shape. The errors on this *highly correlated* set of configurations are dominated by the large variance of the small-scale mode Δk and are typically slightly larger than 10 per cent. Still, the one-loop approximation for the Gaussian case breaks down already around $k = 0.15\,h\,\mathrm{Mpc}^{-1}$ at redshift zero. The SC01 formula instead shows the same discrepancy noted above around $k \sim 0.1\,h\,\mathrm{Mpc}^{-1}$ while it provides a better fit to the data at larger k. At higher redshift, however, PT fares better than the fitting formula. The limitation of the one-loop prediction for the Gaussian case is also apparent in the corrections due to non-Gaussianity. However, the theoretical prediction for the *ratio* $B_{\rm NG}/B_{\rm G}$ is in remarkable agreement with the data (third row of Fig. 5). Note that the large-k limit in this set of configurations does not correspond to the more common 'squeezed' limit, obtained fixing two sides of the triangle and reducing the third one, so we do not expect an increase in the non-Gaussian component, since at larger k we are probing smaller scales and the suppression due to the transfer function is larger. Nevertheless, the non-Gaussian corrections are relatively large for this set of configuration, ranging from 10 to 30 per cent and growing with redshift. This triangle shape is, among those we consider, most directly comparable to the measurements of Nishimichi et al. (2009) at redshift $z = 0.5$ and in particular to the central panels of their fig. 3. Our errors are consistent with theirs, and the agreement between our data points and tree-level PT at $z = 0.5$ is also reasonable.

In the last two figures, we consider generic scalene triangles for which the length of two sides k_1 and k_2 is held fixed while the angle θ between them (and therefore the length of the third side) is varied. Such a set of triangular configurations is useful to illustrate the shape dependence of the bispectrum as it includes collapsed, flattened and almost equilateral triangles depending on the choice of k_1 and k_2. To further isolate the shape dependence of the matter bispectrum from its scale dependence, it is convenient to introduce the *reduced* bispectrum $Q(k_1, k_2, k_3)$ defined as

$$Q \equiv \frac{B(k_1, k_2, k_3)}{P(k_1)P(k_2) + P(k_1)P(k_3) + P(k_2)P(k_3)}. \tag{34}$$

In Figs 6 and 7, we will show the reduced bispectrum in the first rows instead of the bispectrum itself. Note that the one-loop predictions for the reduced bispectrum are computed from a proper expansion of the denominator in terms of the one-loop expression for the power spectrum (see Sefusatti 2009, for details). The quantities shown in the other rows are the same as before. A second difference with the previous plots is the fact that the data points are plotted as a function of the effective angle θ defined in equation (33) (see Section 3.1).

In Fig. 6, we consider the specific case $k_1 = 0.094\,h\,\mathrm{Mpc}^{-1}$ and $k_2 = 1.5k_1$. For these configurations, $\theta \lesssim 0.6\pi$ implies that all three sides are larger than $0.1\,h\,\mathrm{Mpc}^{-1}$. On these scales, the agreement of the one-loop predictions with the measurements at $z = 0$ is poor, as is evident from the first plots on the second row. Errors on the bispectrum mean are typically of the order of 3 per cent. At redshift $z \gtrsim 1$, however, the theoretical predictions fall within the errors. Rather puzzling is, however, the relatively poor agreement at $z = 2$, in fact already present in the previous plots and perhaps related to small discrepancy between RPT predictions and simulations in the power spectrum case. The prediction for the relative effect of primordial non-Gaussianity, which is about 3 per cent at all redshift, is in good agreement with the data regardless of the triangle shape (third row). The apparent bump shown in these plots results from the low values of the 'Gaussian' bispectrum for nearly equilateral triangles evident from the plots in the first row, rather than a non-Gaussian feature. Instead, the larger non-Gaussian signal expected for triangles approaching the squeezed limit is observable in the 'difference' plots on the fourth row for $\theta \simeq \pi$.[1] Notably, the same feature also appears in the component B^{II}_{112} dependent on the initial trispectrum T_0 (last row).

Similar results are found for a second set of triangles where the two sides are now much closer in size, $k_1 = 0.14\,h\,\mathrm{Mpc}^{-1}$ and $k_2 = 0.15\,h\,\mathrm{Mpc}^{-1}$ (see Fig. 7). In this case, however, the configurations are very close to equilateral for $\theta \simeq 0.6\pi$. As a result, we observe at $z = 0$ the same discrepancy between PT and simulations than that seen in Fig. 3 at small scales. This disagreement is also apparent in the plot of the reduced bispectrum. The non-Gaussian correction is typically of the order of 3 per cent, but it increases significantly in the squeezed limit $\theta \to \pi$. This behaviour of the linear and non-linear components due to primordial non-Gaussianity is also evident in the fourth row showing the difference $B_{\rm NG} - B_{\rm G}$.

5 CONCLUSIONS

A rather surprising effect of local primordial non-Gaussianity on the large-scale clustering properties of biased objects has been observed in various numerical studies over the last years (Dalal et al. 2008; Desjacques et al. 2009; Grossi et al. 2009; Pillepich et al. 2010).

[1] When the 'direction' of the three wavevectors with the sum equal to zero, i.e. $\boldsymbol{k}_1 + \boldsymbol{k}_1 + \boldsymbol{k}_3 = 0$, is taken into account it easy to see that the 'squeezed' limit is obtained for $\theta \to \pi$, rather than $\theta \to 0$ as one might naïvely think just considering the triangle defined by the wavenumber magnitudes alone.

© 2010 The Authors. Journal compilation © 2010 RAS, MNRAS **406,** 1014–1028

These results attracted a great deal of attention as they showed that measurements of the power spectrum of galaxies and quasars from current data sets can lead to constraints on the local non-Gaussian parameter $f_{\rm NL}$ comparable to those of CMB observations (Slosar et al. 2008; Desjacques & Seljak, 2010b). Previous work assumed that the main effect of primordial non-Gaussianity is limited to an extra contribution to the matter and galaxy bispectrum. Still, even under such an incorrect but 'conservative' assumption, it has been shown that future large-volume redshift surveys will reach a sensitivity to a non-zero $f_{\rm NL}$ comparable to or better than the CMB bispectrum (Scoccimarro et al. 2004; Sefusatti & Komatsu 2007). The inclusion of the non-Gaussian bias in the analysis of the galaxy bispectrum or, better, in a combined analysis of the power spectrum and bispectrum, is desirable to reliably assess the potentiality of forthcoming surveys of the large-scale structure.

As a first step in this direction, we have measured the matter bispectrum for the main classes of triangle shape using a set of large-volume N-body simulations seeded with Gaussian and non-Gaussian initial conditions of the local type. We focused on mildly non-linear scales, $0.02 \lesssim k \lesssim 0.3\,h\,{\rm Mpc}^{-1}$, presented a wide choice of triangular configurations of different shapes and obtained a determination of the bispectrum with an overall error of the order of 3-4 per cent. Of particular interest in this range of scales are the non-linear corrections induced by gravitational instability *due* to non-Gaussian initial conditions as they generate an additional non-Gaussian signal on top of the primordial component. For a non-linear parameter $f_{\rm NL} = 100$, we found that the amplitude of these corrections ranges from 3–4 per cent for generic triangle configurations up to 20–30 per cent for 'squeezed' configurations where we expect most of the signal for local non-Gaussianity. We quantified these corrections with the aid of the ratio and the difference between the non-Gaussian and the Gaussian bispectra. Our set of eight different realizations of those models ensure that our results are robust to sampling variance. We considered simulation snapshots at redshifts $z = 0, 1$ and 2. Overall, we found that the magnitude of the correction induced by non-Gaussian effects is similar regardless the scale and the redshift. This is due to a compensation between the primordial component that decreases with time, on the one hand, and the contribution from non-linear structure growth that increases with time, on the other hand.

We compared our results with the predictions of Eulerian PT, both at tree-level and at one-loop (Sefusatti 2009). As expected, and similar to what happens for Gaussian initial conditions, the tree-level approximation fails at relatively large scales, $k \sim 0.05$–$0.1\,h\,{\rm Mpc}^{-1}$, even at high redshift. One-loop corrections extend significantly the predictive power of PT down to mildly non-linear scales $k \sim 0.3\,h\,{\rm Mpc}^{-1}$ at redshift $z \gtrsim 1$, similar to the case of the power spectrum analysed by Jeong & Komatsu (2006). They describe, in fact, the matter bispectrum measured in simulations at the few per cent level, with an even better agreement with respect to the 'relative' effect of primordial non-Gaussianity on the Gaussian bispectrum. Furthermore, they also show a good qualitative agreement with simulations at redshift zero.

ACKNOWLEDGMENTS

We thank Roman Scoccimarro and Francis Bernardeau for useful comments. ES acknowledges support by the French Agence National de la Recherche (ANR) under grant BLAN07-1-212615 and by the European Commission under the Marie Curie Inter European Fellowship and he is grateful to the Institute for Theoretical Physics of the University of Zürich for hospitality during the completion of this project. MC would like to thank the Institut de Physique Théorique of CEA-Saclay for hospitality and acknowledges support from the Spanish Ministerio de Ciencia y Tecnologia (MEC) through the Juan de la Cierva programme. VD would like to thank the Institut d'Astrophysique de Paris for hospitality during the final stages of this work and the Swiss National Foundation (under contract no. 200021-116696/1) for support.

REFERENCES

Afshordi N., Tolley A. J., 2008, Phys. Rev. D, 78, 123507
Bartolo N., Komatsu E., Matarrese S., Riotto A., 2004, Phys. Rep., 402, 103
Bartolo N., Beltran Almeida J. P., Matarrese S., Pietroni M., Riotto A., 2009, preprint (arXiv:0912.4276)
Bernardeau F., Colombi S., Gaztañaga E., Scoccimarro R., 2002, Phys. Rep., 367, 1
Bernardeau F., Crocce M., Scoccimarro R., 2008, Phys. Rev. D, 78, 103521
Byrnes C. T., Choi K.-Y., 2010, preprint (arXiv:1002.3110)
Carbone C., Verde L., Matarrese S., 2008, ApJ, 684, L1
Chen X., 2010, preprint (arXiv:1002.1416)
Crocce M., Scoccimarro R., 2006a, Phys. Rev. D, 73, 063519
Crocce M., Scoccimarro R., 2006b, Phys. Rev. D, 73, 063520
Crocce M., Scoccimarro R., 2008, Phys. Rev. D, 77, 023533
Crocce M., Pueblas S., Scoccimarro R., 2006, MNRAS, 373, 369
Dalal N., Doré O., Huterer D., Shirokov A., 2008, Phys. Rev. D, 77, 123514
Desjacques V., Seljak U., 2010a, Phys. Rev. D, 81, 023006
Desjacques V., Seljak U., 2010b, preprint (arXiv:1003.5020)
Desjacques V., Seljak U., Iliev I. T., 2009, MNRAS, p. 631
Eisenstein D. J., Hu W., 1998, ApJ, 496, 605
Fry J. N., 1984, ApJ, 279, 499
Gangui A., Lucchin F., Matarrese S., Mollerach S., 1994, ApJ, 430, 447
Giannantonio T., Porciani C., 2010, Phys. Rev. D, 81, 063520
Grossi M., Branchini E., Dolag K., Matarrese S., Moscardini L., 2008, MNRAS, 390, 438
Grossi M., Verde L., Carbone C., Dolag K., Branchini E., Iannuzzi F., Matarrese S., Moscardini L., 2009, MNRAS, 398, 321
Guo H., Jing Y. P., 2009, ApJ, 698, 479
Hamilton A. J. S., Kumar P., Lu E., Matthews A., 1991, ApJ, 374, L1
Hou Y. H., Jing Y. P., Zhao D. H., Börner G., 2005, ApJ, 619, 667
Jeong D., Komatsu E., 2006, ApJ, 651, 619
Jeong D., Komatsu E., 2009, ApJ, 703, 1230
Kamionkowski M., Verde L., Jimenez R., 2009, J. Cosmol. Astropart. Phys., 1, 10
Komatsu E., Spergel D. N., 2001, Phys. Rev. D, 63, 063002
Komatsu E. et al., 2009a, Astro2010: The Astronomy and Astrophysics Decadal Survey, Science White Papers, 158
Komatsu E. et al., 2009b, ApJS, 180, 330
Komatsu E. et al., 2010, preprint (arXiv:1001.4538)
Lam T. Y., Sheth R. K., 2009, MNRAS, 398, 2143
Lam T. Y., Sheth R. K., Desjacques V., 2009, MNRAS, 399, 1482
Lewis A., Challinor A., Lasenby A., 2000, ApJ, 538, 473
Liguori M., Sefusatti E., Fergusson J. R., Shellard E. P. S., 2010, preprint (arXiv:1001.4707)
McDonald P., 2008, Phys. Rev. D, 78, 123519
Maggiore M., Riotto A., 2009, preprint (arXiv:0903.1251)
Matarrese S., Pietroni M., 2007, J. Cosmol. Astropart. Phys., 6, 26
Matarrese S., Verde L., 2008, ApJ, 677, L77
Nishimichi T., Taruya A., Koyama K., Sabiu C., 2009, preprint (arXiv:0911.4768)
Pan J., Coles P., Szapudi I., 2007, MNRAS, 382, 1460
Peacock J. A., Dodds S. J., 1996, MNRAS, 280, L19
Pietroni M., 2008, J. Cosmology Astropart. Phys., 10, 36
Pillepich A., Porciani C., Hahn O., 2010, MNRAS, 402, 191
Salopek D. S., Bond J. R., 1990, Phys. Rev. D, 42, 3936
Salopek D. S., Bond J. R., 1991, Phys. Rev. D, 43, 1005
Scoccimarro R., 1997, ApJ, 487, 1

Scoccimarro R., 1998, MNRAS, 299, 1097
Scoccimarro R., 2000, ApJ, 544, 597
Scoccimarro R., Couchman H. M. P., 2001, MNRAS, 325, 1312
Scoccimarro R., Colombi S., Fry J. N., Frieman J. A., Hivon E., Melott A., 1998, ApJ, 496, 586
Scoccimarro R., Sefusatti E., Zaldarriaga M., 2004, Phys. Rev. D, 69, 103513
Sefusatti E., 2009, Phys. Rev. D, 80, 123002
Sefusatti E., Komatsu E., 2007, Phys. Rev. D, 76, 083004
Sefusatti E., Crocce M., Pueblas S., Scoccimarro R., 2006, Phys. Rev. D, 74, 023522
Sefusatti E., Liguori M., Yadav A. P. S., Jackson M. G., Pajer E., 2009, J. Cosmol. Astropart. Phys., 12, 22
Seljak U., 2009, Phys. Rev. Lett., 102, 021302
Slosar A., 2009, J. Cosmol. Astropart. Phys., 3, 4
Slosar A., Hirata C., Seljak U., Ho S., Padmanabhan N., 2008, J. Cosmol. Astropart. Phys., 8, 31
Smith R. E. et al., 2003, MNRAS, 341, 1311
Smith R. E., Sheth R. K., Scoccimarro R., 2008, Phys. Rev. D, 78, 023523
Springel V., 2005, MNRAS, 364, 1105
Taruya A., Koyama K., Matsubara T., 2008, Phys. Rev. D, 78, 123534
Verde L., Matarrese S., 2009, ApJ, 706, L91
Verde L., Wang L., Heavens A. F., Kamionkowski M., 2000, MNRAS, 313, 141
Zel'Dovich Y. B., 1970, A&A, 5, 84

This paper has been typeset from a TEX/LATEX file prepared by the author.